

Magnetic Dirac fermions and Chern insulator supported on pristine silicon surfaceHuixia Fu,¹ Zheng Liu,² Chao Lian,¹ Jin Zhang,¹ Hui Li,¹ Jia-Tao Sun,^{1,*} and Sheng Meng^{1,3,*}¹*Beijing National Laboratory for Condensed Matter Physics and Institute of Physics, Chinese Academy of Sciences, Beijing 100190, People's Republic of China*²*Institute for Advanced Study, Tsinghua University, Beijing 100084, People's Republic of China*³*Collaborative Innovation Center of Quantum Matter, Beijing 100190, People's Republic of China*

(Received 10 April 2016; published 18 July 2016)

Emergence of ferromagnetism in nonmagnetic semiconductors is strongly desirable, especially in topological materials because of the possibility of achieving the quantum anomalous Hall effect. Based on first-principles calculations, we propose that for Si thin film grown on metal substrate, the pristine Si(111)- $\sqrt{3} \times \sqrt{3}$ surface with a spontaneous weak reconstruction has a strong tendency toward ferromagnetism and nontrivial topological properties, characterized by spin-polarized Dirac-fermion surface states. In contrast to conventional routes relying on introduction of alien charge carriers or specially patterned substrates, the spontaneous magnetic order and spin-orbit coupling on the pristine silicon surface together give rise to the quantized anomalous Hall effect with a finite Chern number $C = -1$. This work suggests opportunities in silicon-based spintronics and quantum computing free from alien dopants or proximity effects.

DOI: [10.1103/PhysRevB.94.035427](https://doi.org/10.1103/PhysRevB.94.035427)**I. INTRODUCTION**

Being able to generate magnetism in semiconducting materials that are not naturally magnetic brings new opportunities to spintronics applications. Recently, the pursuit of ferromagnetic ordering in the two-dimensional (2D) d^0 materials has attracted wide attention owing to intriguing physical phenomena and tremendous potential applications. In graphene and BN, besides directly doping transition metal elements, the magnetic moments can also be induced by introducing nonmagnetic adatoms [1], vacancy defects, structural distortions [2–4], edge engineering [5–7], and the proximity with ferromagnetic substrates [8]. However, these dopants and defects often induce rather localized magnetic moments; robust long-range ordered ferromagnetism can rarely be obtained in theoretical proposals and experimental measurements [9–14].

Silicon is the most popular d^0 element for semiconductors. The intrinsic ferromagnetism in silicon-based materials could hold great promise for new magnetoelectric effects and nanoscale spintronics that are naturally compatible with the current silicon industry. A prototypical approach to achieve magnetism is to introduce alien atoms onto Si(111) [15–20]. Numerous works have demonstrated the complex spin patterns in Si(111) covered with 1/3 monolayer Sn/Pb atoms, which were attributed to strong electronic correlation induced by adatoms [15–19]. Moreover, Erwin *et al.* reported long-range spin polarization at graphitic steps on a family of vicinal silicon surfaces [20]. Despite the fact that ferromagnetism is believed to originate intrinsically from silicon surfaces, these stepped surfaces have to be stabilized by a small amount of extrinsic gold atoms. Novel properties of Si(111) surfaces in addition to magnetism have also been widely explored [21–23]. Wang *et al.* proposed that a 1/3 monolayer of halogen adatoms on Si(111) can create anisotropic Dirac bands [21]. Studies have reported p -band-element X -decorated Au/Si(111) surfaces

as a promising prototype for larger-gap topological states [22]. The quantum anomalous Hall (QAH) states were also predicted in W/Cl-covered Si(111) systems [23]. However, in all these proposals, alien elements are always necessary to give rise to the magnetic and topological orders mentioned above, thus bringing additional difficulties in controlled doping and surface stability. To date, long-range ordered magnetic states in pristine silicon systems have not been reported either in experiment or theory, and challenges remain in achieving topological electronic structures simultaneously.

In this letter, we propose that ferromagnetism can emerge on weakly reconstructed pure Si(111)- $\sqrt{3} \times \sqrt{3}$ R30° surfaces (hereafter designated as Si- $\sqrt{3}$ surface) by first-principles calculations. This state breaks time-reversal symmetry and is characterized by spin-polarized Dirac subbands with partially filled p_z orbitals, originating from the interplay between spontaneous surface reconstruction and magnetic instability. More remarkably, we find that a band gap of 15 meV is opened up by spin-orbit coupling (SOC) interactions, resulting in a nontrivial QAH state characterized by a Chern number of $C = -1$ and chiral edge states. In contrast to conventional magnetic topological insulators such as doped dilute magnetic semiconductors and tetradymite semiconductors [24], the spontaneous reconstructed Si- $\sqrt{3}$ surface with spin-polarized nontrivial topological bands may serve as a new pathway to realize the QAH effect [8,23–25], without introduction of foreign magnetic impurities or substrates. The proposed Si- $\sqrt{3}$ surface can be prepared by epitaxial growth of Si thin film on metal substrate under low-temperature conditions in a controllable way to remove other competing phases; therefore, the surface ferromagnetism could be experimentally accessible. However, we note that previous reports about “multilayer silicene” on Ag substrate with comparable surface structures have not been unambiguously explained by the model studied here; adatom structures with silver (or other impurities) may account for the observed periodicity [26]. Moreover, the low stability may make the surface reactive to unintended surface contamination, which may easily destroy the fragile electronic structure.

*Authors to whom correspondence should be addressed: jtsun@iphy.ac.cn; smeng@iphy.ac.cn

II. COMPUTATIONAL METHODS

The first-principles calculations were performed using the Perdew-Burke-Ernzerhof (PBE) functional [27] in the Vienna *Ab initio* Simulation Package (VASP) [28]. Projector-augmented wave (PAW) pseudopotentials were applied with an energy cutoff at 400 eV. The Brillouin zone was sampled with an $11 \times 11 \times 1$ Monkhorst-Pack k -mesh. The Si(111) slabs of three to seven silicon layers with a surface lattice constant of 6.67 \AA were chosen with a vacuum region $\geq 15 \text{ \AA}$. The silicon atoms on the bottom layer were saturated by hydrogen atoms. The atomic geometry was optimized until the force on each atom was less than 0.01 eV \AA^{-1} . Beyond the PBE functional, the screened exchange hybrid density functional by Heyd-Scuseria-Ernzerhof (HSE06) [29,30] was also adopted to confirm the electronic structures. To describe the spin-polarized Dirac-type surface state and make the Chern number calculation computationally efficient, an effective tight-binding (TB) Hamiltonian was constructed by projecting Bloch states onto maximally localized Wannier functions (MLWFs) using the VASP2WANNIER90 interface [31,32]. Then, a dense k mesh of $600 \times 600 \times 1$ over the entire Brillouin zone was employed to ensure the convergence of the integral.

III. RESULTS AND DISCUSSION

The atomic structure of the Si(111) slab with an in-plane $\sqrt{3} \times \sqrt{3} \text{ R}30^\circ$ supercell was first optimized by performing non-spin-polarized calculations as shown in Figs. 1(a) and 1(b). We found that weak reconstruction of a rhombic Si- $\sqrt{3}$ surface without bond breaking spontaneously takes place on all Si(111) slabs with ≥ 3 silicon layers. Here, $1/3$ of the three-coordinated Si_A (green) atoms on the Si- $\sqrt{3}$ surface are 1.2 \AA higher than the four-coordinated Si_C (orange) atoms. The remaining $2/3$ of the three-coordinated Si_B (red) atoms with one dangling bond are nearly flat lying at a height of $\sim 0.24 \text{ \AA}$ above Si_C atoms. The Si_B atoms form a superhexagonal honeycomb lattice with a $\sqrt{3} \times \sqrt{3} \text{ R}30^\circ$ periodicity with respect to the ideal Si(111)- 1×1 lattice. Compared with the sp^3 bonding features of ideal bulk Si(111), the low-buckled Si- $\sqrt{3}$ surface, consisting of only two Si_B atoms within the $\sqrt{3} \times \sqrt{3} \text{ R}30^\circ$ superlattice, closely resembles a perfect planar graphene structure. One expects that the unsaturated p_z orbital from each Si_B atom might form sp^2 hybridization,

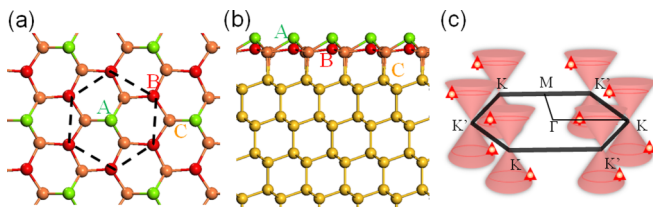


FIG. 1. Top view (a) and side view (b) of Si- $\sqrt{3}$ surface. The green, red, and orange balls, respectively, denote three types of silicon atoms: Si_A (highest), Si_B (lower), Si_C (lowest) on the surface layer. Yellow spheres are the bulk Si atoms. The bottom Si layer is saturated by H atoms. (c) Schematic diagram of spin-polarized Dirac cones around the Fermi level in the first Brillouin zone.

giving rise to a Dirac cone in the band gap region of bulk states.

The representative electronic band structure of the Si- $\sqrt{3}$ surface in the nonmagnetic (NM) phase is shown in Fig. 2(a). Indeed, a Dirac-like state (orange lines) around the Fermi level can be easily distinguished from the bulk states (blue shadow areas). The corresponding density of states (DOS), as well as the orbital projected DOS [Fig. 2(b)], exhibits a partially filled peak with a band width of 0.2 eV around the Fermi level, mainly originating from the p_z orbitals of the Si_B surface atoms. This fact indicates that the electronic origin of the Dirac-like state is from delocalized π bonds attributed to the planar superhexagonal bond topology of the Si_B atoms. Furthermore, this partially filled Dirac state with a narrow band width, which is characterized as a sharp van Hove singularity in DOS, suggests a strong interaction among the electrons lying at the Fermi level. It is likely to invoke Stoner magnetic instabilities and result in a magnetic ground state accompanied by spin-dependent Dirac states around the Fermi level.

Naturally, we then considered the potential long-range magnetic orders in the surface states of the Si- $\sqrt{3}$ surface. Both ferromagnetic (FM) and antiferromagnetic (AFM) ordering have been considered (Supplemental Material Fig. S1 [33]). Interestingly, we found that the Si- $\sqrt{3}$ surface favors FM spin ordering, with a calculated magnetic moment of $1 \mu_B$ per $\sqrt{3}$ unit cell. This implies that each pair of Si_B atoms per $\sqrt{3}$ unit cell shares a single π -bonding electron, while the Si_A atom is fully saturated with a lone pair of two electrons, due to the symmetry breaking between Si_A and Si_B atoms in the $\sqrt{3}$ unit cell. In contrast, the initial AFM spin configuration will spontaneously relax into the NM phase. The favorable FM configuration was further verified in the larger $2\sqrt{3} \times 2\sqrt{3} \text{ R}30^\circ$ and 3×3 supercells to eliminate the potential errors induced by small cell sizes. Meanwhile, the priority of the FM phase over both NM and AFM cases was found for all Si(111) slabs of various thickness as long as the surface reconstruction occurs. Our spin-polarized calculations predict that the FM structure is 91 meV more stable than the NM phase per $\sqrt{3}$ supercell. The qualitative results have also been reproduced by the HSE06 hybrid functional, which is more accurate to describe the sp hybridization. The HSE06 functional presents an even larger energy difference of 204 meV per $\sqrt{3}$ cell between the FM and NM phases. Coincident with the foregoing assumption, the calculated band structure and DOS for the FM structure exhibit two spin-polarized Dirac cones with an energy splitting of 0.39 eV at the K point, as shown in Figs. 2(c) and 2(d).

It is noteworthy that the spin-majority channel gives rise to a zero-gap semiconductor, whereas the spin-minority channel displays an indirect semiconducting band gap of 0.44 eV , demonstrating a unique spin semiconductor feature, as illustrated in Supplemental Material Fig. S2 [33]. Since the Fermi velocity v_F is a key parameter to describe the fundamental characters of Dirac materials, the magnified spin-majority Dirac cone at the energy window from -0.3 eV to 0.4 eV obtained from both PBE and HSE06 functional is plotted in Fig. S3 [33]. We see the sharp feature of the Dirac band is very similar using different functionals. The Fermi velocity v_F is $0.47 \times 10^6 \text{ m s}^{-1}$ by fitting the linear dispersion branch of the

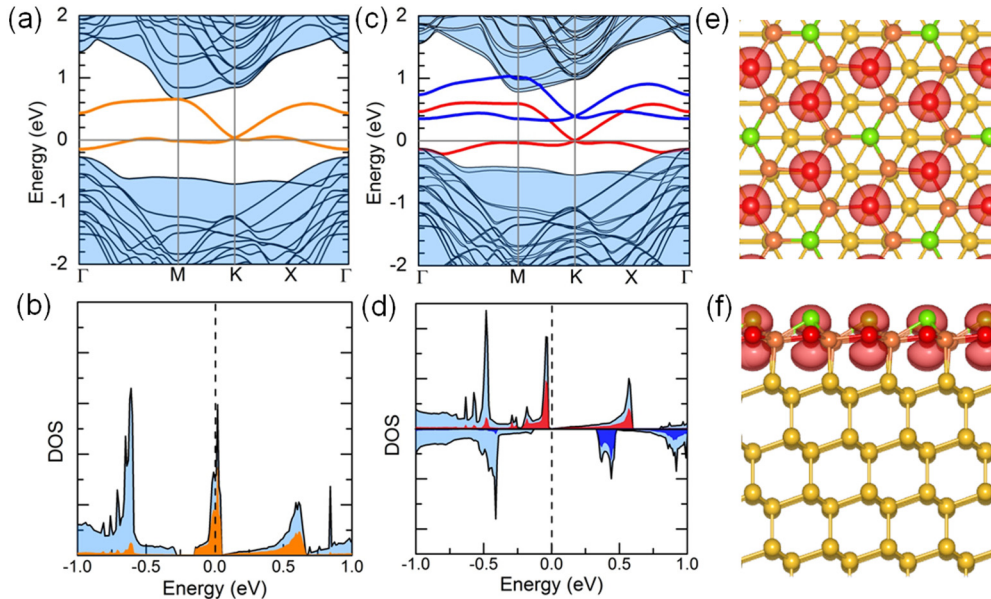


FIG. 2. Band structures for the Si- $\sqrt{3}$ surface in the NM (a) and FM phase (c). The shadow regions are the bulk states and the flat band from Si_A atoms. The yellow, red, and blue lines are the Dirac bands from the states of Si_B atoms. (b, d) The corresponding DOS for the Si thin films. The yellow, red, and blue regions correspond to the projected DOS on Si_B atoms. (e, f) Top and side view of the spin density distribution at the isosurface level of $0.002 \text{ e}^- \text{ \AA}^{-3}$.

valence band from the HSE06 function, which is comparable to the value of 10^6 m s^{-1} for electrons in suspended graphene [34]. The spin density distribution displayed in Figs. 2(e) and 2(f) demonstrates that the ferromagnetic feature can be mostly attributed to the p_z orbital of the superhexagonal Si_B pattern, which has the largest contribution to the spin-polarized Dirac states [Fig. 2(d)].

The favorable FM phase over the NM state on the Si- $\sqrt{3}$ surface signifies the magnetic instability predicted above, which can be understood from the Stoner criterion in the noninteracting regime [35]. One can determine whether $N(E_F)U > 1$ applies, where $N(E_F)$ is the DOS at the Fermi level in the non-spin-polarized state, and U is a measure of the strength of the exchange interaction between the two Dirac cones in the spin-polarized state. Substituting with the values from density functional theory (DFT) calculations, we obtain $N(E_F)U = 6.53/(\text{eV} \cdot \text{unit cell}) \times 0.39 \text{ eV} = 2.5 > 1$. In this simple Stoner model, the condition for the emergence of FM order is fulfilled, suggesting a spin-polarized state might take place on the Si- $\sqrt{3}$ surface.

Being a quick predictive tool, Stoner theory is in fact not always successful due to the absence of many body interactions [36]. In order to understand the underlying spin exchange, one needs also to evaluate the electron-electron interaction not captured within the noninteracting regime. Via transforming the Bloch wave function of the spin-polarized Dirac subbands into real space on a Wannier basis, we obtain the single orbital hopping in the mean field framework $H_0 = \sum_{i,j} t_{ij} c_i^\dagger c_j$, where i, j denote the positions of different Si_B atoms, and t_{ij} denotes the electron hopping between them. The obtained nearest neighbor (NN) hopping amplitude t_1 is -52.6 meV in the Wannier basis. In the representation of the same Wannier basis, the Hamiltonian for the dominant electron-electron interaction

can be expressed as [37],

$$H_{\text{int}} = \tilde{U}_0 \sum_i n_{i\downarrow} n_{i\uparrow} + \tilde{U}_1 \sum_{\langle ij \rangle} n_i n_j + \tilde{J}_{\text{ex}} \sum_{\langle ij \rangle \alpha} c_{i,\alpha}^\dagger c_{j,-\alpha}^\dagger c_{i,-\alpha} c_{j,\alpha}, \quad (1)$$

where $\langle ij \rangle$ and α denote the NN pairs and spin index, respectively. $\tilde{U}_0, \tilde{U}_1, \tilde{J}_{\text{ex}}$ are respectively the on-site Hubbard repulsion, NN direct repulsion, and NN direct exchange (see Supplementary Material [33]). Sampling the Wannier basis using Monte Carlo method, we obtain $\tilde{U}_0 = 6.404 \text{ eV}$, $\tilde{U}_1 = 2.461 \text{ eV}$, and $J_{\text{ex}} = 4.5 \text{ meV}$. The condition $t_1 \ll \tilde{U}_0$ will push the Si- $\sqrt{3}$ surface toward a strongly localized spin state. The positive value $J_{\text{ex}} = 4.5 \text{ meV}$ suggests a ferromagnetic phase with a Curie temperature up to 52 K.

With a staggered magnetic flux emerging from the spin-polarized Dirac fermion and the intrinsic SOC, the Si- $\sqrt{3}$ surface may exhibit the QAH effect featuring nontrivial Chern numbers. To illustrate this feature, we interpolated the spin-polarized Dirac bands based on the atom-centered p_z -like MLWFs with the SOC effect turned on. The Wannier-interpolated energy bands are in excellent agreement with the DFT results around the Fermi level [Fig. 3(a)]. Furthermore, a small band gap of $\sim 4.5 \text{ meV}$ (15 meV) with PBE (HSE06) functional is opened at the touching point of the spin-majority Dirac cone. The SOC gap value is higher than that of monolayer silicene (1.55 meV), which is the only pristine-silicon-based topological insulator that has been proposed [38]. When the Fermi level lies inside this energy gap, the insulating state could be a Chern insulator, which can be

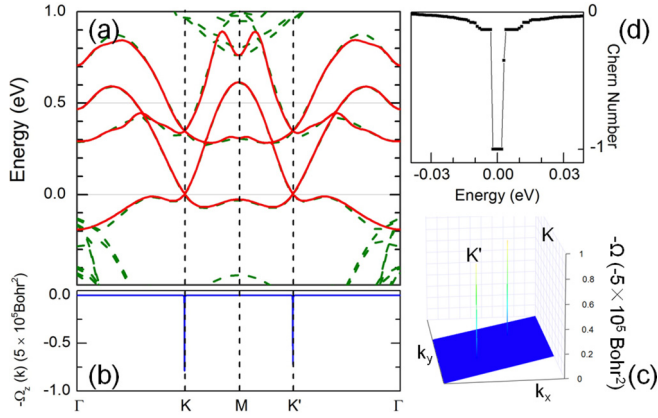


FIG. 3. (a) Energy band structure for the Si- $\sqrt{3}$ surface calculated by DFT (green dashed line) and fitted by a Wannier basis set (red line). (b) The Berry curvature for the valence bands below the Fermi level along the high-symmetry direction. (c) The 2D distribution of Berry curvature for the occupied bands in momentum space. (d) The energy dependence of the first Chern number around the quantized conductance plateau.

characterized by the first Chern number \mathcal{C} calculated by,

$$\mathcal{C} = \frac{1}{2\pi} \sum_n \int_{BZ} d^2k \Omega_n, \quad (2)$$

where Ω_n is the momentum-space Berry curvature for the n th band [39–41], given as

$$\Omega_n(k) = - \sum_{n' \neq n} \frac{2\text{Im}\langle \psi_{nk} | v_x | \psi_{n'k} \rangle \langle \psi_{n'k} | v_y | \psi_{nk} \rangle}{(\epsilon_{n'} - \epsilon_n)^2}. \quad (3)$$

The summation is over all occupied valence bands in the first Brillouin zone, and $v_{x(y)}$ is the velocity operator along the $x(y)$ direction. The absolute value of \mathcal{C} corresponds to the number of gapless chiral edge states along the edges of the Si- $\sqrt{3}$ surface.

The Berry curvature $\Omega_n(k)$ along the high-symmetry direction Γ - K - M - K' - Γ shows two sharp spikes of the same sign located right at the K and K' points [Fig. 3(b)]. The even function of $\Omega_n(k)$ for all the occupied states can be clearly seen in the two-dimensional distribution in the entire Brillouin zone, which also shows vanishing $\Omega_n(k)$ away from both valleys [Fig. 3(c)]. By integrating the Berry curvature $\Omega_n(k)$ in the entire Brillouin zone, we obtain the Chern number $\mathcal{C} = -1$, indicating one nontrivial edge state. As expected from the nonzero Chern number, the anomalous Hall conductivity shows a quantized charge Hall plateau of $\sigma_{xy} = \mathcal{C}e^2/h$ when the Fermi level is located in the insulating gap of the spin-majority Dirac cone [Fig. 3(d)]. Via the HSE06 functional, the width of the Hall plateau will increase to 15 meV, which is readily accessible in experimental conditions.

The existence of topologically protected chiral edge states is one of the most important signatures of the QAH effect [Fig. 4(a)]. To further reveal the nontrivial topological nature of the Si- $\sqrt{3}$ surface, we calculated the nanoribbon structure having a width of 200 zigzag silicon chains, ignoring the

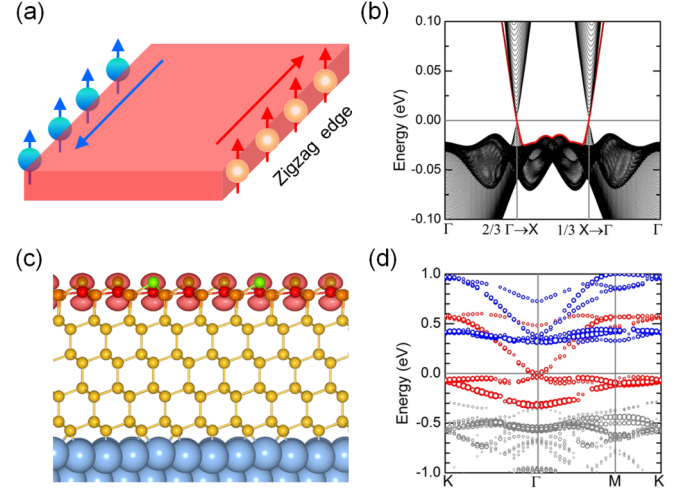


FIG. 4. (a) Schematic illustration of the quantum anomalous Hall conductivity σ_{xy}^H . The spin-polarized Hall currents along two edges are shown by blue and red color. (b) The tight-binding band structure for a Si- $\sqrt{3}$ nanoribbon with a width of 200 zigzag Si chains. The quantized edge states are shown by red lines. (c) Atomic structure and spin distribution of five-layer Si(111) films with $\sqrt{3}$ surface on Ag(111) substrate. The lattice constant of the supercell is 11.56 Å. The spin density distribution at the isosurface level of $0.002 \text{ e}^- \text{ \AA}^{-3}$ is shown. (d) Projected band structure on the topmost Si atomic layer for the five-layer Si(111) films on silver substrate. The red and blue dots represent spin-majority and spin-minority Dirac states from Si_B atoms, respectively. The sizes of dots denote the weight of contribution.

effects of edge reconstruction, using a tight binding model built on the Wannier basis described above. As shown in Fig. 4(b), we clearly see that the nontrivial edge states (red line) connecting the valence and conduction bands cross the insulating gap of the spin-majority Dirac cone. The appearance of only one chiral edge state is consistent with the calculated Chern number $\mathcal{C} = -1$, confirming the nontrivial topological nature of the Si- $\sqrt{3}$ surface. The spin-polarized Dirac-fermion-mediated topological characters suggest the pure silicon surface proposed here is an intrinsic magnetic topological insulator, holding the potential to generate the QAH effect.

Recently, the Si(111) thin films with $\sqrt{3}$ surface reconstruction have been successfully fabricated on silver substrates via molecular beam epitaxy (MBE) grown in an ultrahigh-vacuum chamber [42,43]. Although the exact surface composition is still under debate [26], the advances in thin film synthesis offer a promising route for experimental realization of the QAH effect based on the Si- $\sqrt{3}$ surface. We also confirm that the magnetism of the Si- $\sqrt{3}$ surface survives in thin films grown on a Ag(111) substrate [Fig. 4(c)]. The calculated magnetic moment of $0.48 \mu_B$ per Si_B atom for the Si- $\sqrt{3}$ surface on silver substrate is slightly less than the value ($0.50 \mu_B/\text{Si}_B$) for the freestanding silicon films, which should be the result of a small amount of charge transfer from the Si film to the Ag substrate. The spin-polarized Dirac surface states can be easily distinguished from the projected band structures displayed in Fig. 4(d). The touching points of two

spin-polarized Dirac cones are located at the Γ point due to the band folding, with an obvious energy splitting of 0.38 eV. The spontaneous intrinsic magnetization survives when the number of silicon layers in the slab is ≥ 3 , where the reconstructed surface is satisfactorily far away from the Ag substrate to eliminate mutual interactions. The direct detection of spin polarization in such a system can be achieved by surface sensitive instruments such as a spin-polarized scanning tunneling microscope, magneto-optic Kerr effect measurement, or superconducting quantum interference devices. Moreover, the surface ferromagnetism discussed here provides a notable electronic feature that can be used to distinguish the pure Si- $\sqrt{3}$ surface from the nonmagnetic Si-Ag alloy phase, suggesting a new way to justify the debated surface composition of multilayer silicene on silver substrate.

Since the Si- $\sqrt{3}$ surface has a weak reconstruction, additional steps might be taken to protect the surface from impurity contamination. Thus, we propose to use monolayer BN with $\sqrt{7} \times \sqrt{7}$ periodicity as a chemically inert layer on the top of the $\sqrt{3}$ structure, which has only a very small lattice mismatch of $< 1\%$, shown in Supplemental Material Fig. S4(a) [33]. The van der Waals (vdW) functional in the vdW-optB88 [44] scheme is used to optimize the vdW packed heterostructure. The minimum vertical distance between the BN and Si films is found to be 3.2 Å, indicating a weak interaction between them. As shown in Supplemental Material Fig. S4(b) [33], the projected band structures on the BN film are completely isolated from the Dirac bands of the Si surface, indicating the spin-polarized Dirac surface states survive under the protection of BN films.

IV. CONCLUSION

In conclusion, we propose that the pristine Si- $\sqrt{3}$ surface is pushed to a magnetic ground state upon spontaneous weak reconstruction. The ferromagnetic state is characterized by the spin-polarized Dirac fermions with a high Fermi velocity of $0.47 \times 10^6 \text{ m s}^{-1}$. More interestingly, the QAH effect can be experimentally accessed on pristine silicon surface due to a nontrivial SOC gap of 15 meV. These results suggest that the pristine Si- $\sqrt{3}$ surface is a potential intrinsic magnetic topological insulator, calling for experimental proofs. We have found that the novel electronic characteristics of spin-polarized Dirac fermions can persist on 1/3 layer H-terminated Si(111) and similar Ge- $\sqrt{3}$ surfaces, implying that the magnetism discussed here is a general phenomenon and would stimulate future design of spintronic and magnetoelectronic devices based on d^0 elements. This work presents a new opportunity to understand magnetism in d^0 -element silicon-based materials and might give rise to broad applications in silicon-compatible spintronic and magnetoelectronic devices.

ACKNOWLEDGMENTS

The authors thank Dr. Feng Liu and Zijing Ding for helpful discussions. This work was supported by the National Basic Research Program of China (Grants No. 2013CBA01600, No. 2015CB921001, and No. 2012CB921403), the Natural Science Foundation of China (Grant No. 61306114), and “Strategic Priority Research Program (B)” of the Chinese Academy of Sciences (Grant No. XDB07030100), Chinese Youth 1000 Talents Program.

-
- [1] D. W. Boukhvalov, M. I. Katsnelson, and A. I. Lichtenstein, *Phys. Rev. B* **77**, 035427 (2008).
 - [2] C. Jin, F. Lin, K. Suenaga, and S. Iijima, *Phys. Rev. Lett.* **102**, 195505 (2009).
 - [3] O. V. Yazyev and L. Helm, *Phys. Rev. B* **75**, 125408 (2007).
 - [4] O. V. Yazyev, *Phys. Rev. Lett.* **101**, 037203 (2008).
 - [5] Y. W. Son, M. L. Cohen, and S. G. Louie, *Nature* **444**, 347 (2006).
 - [6] D. Yu, E. M. Lupton, H. J. Gao, C. Zhang, and F. Liu, *Nano Res.* **1**, 497 (2008).
 - [7] O. V. Yazyev and M. I. Katsnelson, *Phys. Rev. Lett.* **100**, 047209 (2008).
 - [8] Z. Wang, C. Tang, R. Sachs, Y. Barlas, and J. Shi, *Phys. Rev. Lett.* **114**, 016603 (2015).
 - [9] J.-H. Chen, L. Li, W. G. Cullen, E. D. Williams, and M. S. Fuhrer, *Nat. Phys.* **7**, 535 (2011).
 - [10] B. Dlubak, M.-B. Martin, C. Deranlot, B. Sertel, S. Xavier, R. Mattana, M. Sprinkle, C. Berger, W. A. D. Heer, F. Petroff, A. Anane, P. Seneor, and A. Fert, *Nature Phys.* **8**, 557 (2012).
 - [11] K. M. McCreary, A. G. Swartz, W. Han, J. Fabian, and R. K. Kawakami, *Phys. Rev. Lett.* **109**, 186604 (2012).
 - [12] R. R. Nair, M. Sepioni, I. L. Tsai, O. Lehtinen, J. Keinonen, A. V. Krashenninnikov, T. Thomson, A. K. Geim, and I. V. Grigorieva, *Nat. Phys.* **8**, 199 (2012).
 - [13] M. B. Lundberg, R. Yang, J. Renard, and J. A. Folk, *Phys. Rev. Lett.* **110**, 156601 (2013).
 - [14] T. Maassen, J. J. van den Berg, E. H. Huisman, H. Dijkstra, F. Fromm, T. Seyller, and B. J. van Wees, *Phys. Rev. Lett.* **110**, 067209 (2013).
 - [15] G. Profeta and E. Tosatti, *Phys. Rev. Lett.* **98**, 086401 (2007).
 - [16] G. Li, P. Höpfner, J. Schäfer, C. Blumenstein, S. Meyer, A. Bostwick, E. Rotenberg, R. Claessen, and W. Hanke, *Nat. Commun.* **4**, 1620 (2013).
 - [17] J.-H. Lee, X.-Y. Ren, Y. Jia, and J.-H. Cho, *Phys. Rev. B* **90**, 125439 (2014).
 - [18] S. Modesti, L. Petaccia, G. Ceballos, I. Vobornik, G. Panaccione, G. Rossi, L. Ottaviano, R. Larciprete, S. Lizzit, and A. Goldoni, *Phys. Rev. Lett.* **98**, 126401 (2007).
 - [19] F. Ronci, S. Colonna, A. Cricenti, and G. Le Lay, *Phys. Rev. Lett.* **99**, 166103 (2007).
 - [20] S. C. Erwin and F. J. Himpsel, *Nat. Commun.* **1**, 58 (2010).
 - [21] Z. F. Wang, and F. Liu, *Phys. Rev. Lett.* **115**, 026803 (2015).
 - [22] B. Huang, K.-H. Jin, H. L. Zhuang, L. Zhang, and F. Liu, *Phys. Rev. B* **93**, 115117 (2016).
 - [23] M. Zhou, Z. Liu, W. Ming, Z. Wang, and F. Liu, *Phys. Rev. Lett.* **113**, 236802 (2014).
 - [24] R. Yu, W. Zhang, H.-J. Zhang, S.-C. Zhang, X. Dai, and Z. Fang, *Science* **329**, 61 (2010).
 - [25] Z. Qiao, W. Ren, H. Chen, L. Bellaiche, Z. Zhang, A. H. MacDonald, and Q. Niu, *Phys. Rev. Lett.* **112**, 116404 (2014).
 - [26] C.-L. Lin, T. Hagino, Y. Ito, K. Kawahara, R. Nagao, M. Aoki, S. Masuda, R. Arafune, M. Kawai, and N. Takagi, *J. Phys. Chem. C* **120**, 6689 (2016).

- [27] J. P. Perdew, K. Burke, and M. Ernzerhof, *Phys. Rev. Lett.* **77**, 3865 (1996).
- [28] G. Kresse and J. Furthmüller, *Phys. Rev. B* **54**, 11169 (1996).
- [29] J. Heyd, G. E. Scuseria, and M. Ernzerhof, *J. Chem. Phys.* **124**, 219906 (2006).
- [30] J. Heyd, G. E. Scuseria, and M. Ernzerhof, *J. Chem. Phys.* **118**, 8207 (2003).
- [31] D. Bilt and N. Marzari, *Comput. Phys. Commun.* **178**, 685 (2008); N. Marzari, A. A. Mostofi, J. R. Yates, I. Souza, and D. Vanderbilt, *Rev. Mod. Phys.* **84**, 1419 (2012).
- [32] C. Franchini, R. Kovik, M. Marsman, S. S. Murthy, J. He, C. Ederer, and G. Kresse, *J. Phys.: Condens. Matter* **24**, 235602 (2012).
- [33] See Supplemental Material at <http://link.aps.org/supplemental/10.1103/PhysRevB.94.035427> for Hubbard model, schemes of spin orientation, additional details on electronic properties, and BN covered Si- $\sqrt{3}$ surface.
- [34] D. C. Elias, R. V. Gorbachev, A. S. Mayorov, S. V. Morozov, A. A. Zhukov, P. Blake, L. A. Ponomarenko, I. V. Grigorieva, K. S. Novoselov, F. Guinea, and A. K. Geim, *Nature Phys.* **7**, 701 (2011).
- [35] E. C. Stoner, *Proc. R. Soc. London A* **165**, 372 (1938); **169**, 339 (1939).
- [36] G. A. Landrum and R. Dronskowski, *Angew. Chem. Int. Ed.* **39**, 1560 (2000).
- [37] Z. Liu, J.-W. Mei, and F. Liu, *Phys. Rev. B* **92**, 165101 (2015).
- [38] C.-C. Liu, W. Feng, and Y. G. Yao, *Phys. Rev. Lett.* **107**, 076802 (2011).
- [39] D. J. Thouless, M. Kohmoto, M. P. Nightingale, and M. den Nijs, *Phys. Rev. Lett.* **49**, 405 (1982).
- [40] M. C. Chang, and Q. Niu, *Phys. Rev. B* **53**, 7010 (1996).
- [41] Y. G. Yao, L. Kleinman, A. H. MacDonald, J. Sinova, T. Jungwirth, D. S. Wang, E. G. Wang, and Q. Niu, *Phys. Rev. Lett.* **92**, 037204 (2004).
- [42] P. D. Padova, C. Ottaviani, C. Quaresima, B. Olivieri, P. Imperatori, E. Salomon, T. Angot, L. Quagliano, C. Romano, A. Vona, M. Muniz-Miranda, A. Generosi, B. Paci, and G. L. Lay, *2D Materials* **1**, 021003 (2014).
- [43] H. X. Fu, L. Chen, J. Chen, J. Qiu, Z. Ding, J. Zhang, K. Wu, H. Li, and S. Meng, *Nanoscale* **7**, 15880 (2015).
- [44] J. Klimeš, D. R. Bowler, and A. Michaelides, *Phys. Rev. B* **83**, 195131 (2011).